Bifractal structure of chromatin in rat lymphocyte nuclei

E. G. Iashina,[1,2] E. Yu. Varfolomeeva,[1] R. A. Pantina,[1] V. Yu. Bairamukov,[1] R. A. Kovalev,[1] N. D. Fedorova,[1] V. Pipich,[3] A. Radulescu,[3] and S. V. Grigoriev[1,2]

[1]*Petersburg Nuclear Physics Institute (PNPI), NRC Kurchatov Institute, Orlova roshcha 1, 188300, Gatchina, Russia*

[2]*Saint-Petersburg State University (SPSU), Ulyanovskaya str. 1, 198504, Saint-Petersburg, Russia*

[3]*Jülich Centre for Neutron Science (JCNS) at Heinz Maier-Leibnitz Zentrum (MLZ) Forschungszentrum Jülich GmbH, Lichtenbergstr. 1, D-85748 Garching, Germany*

(Received 4 October 2021; accepted 29 November 2021; published 22 December 2021)

The small-angle neutron scattering (SANS) on the rat lymphocyte nuclei demonstrates the bifractal nature of the chromatin structural organization. The scattering intensity from rat lymphocyte nuclei is described by power law Q^{-D} with fractal dimension approximately 2.3 on smaller scales and 3 on larger scales. The crossover between two fractal structures is detected at momentum transfer near 10^{-1} nm^{-1}. The use of contrast variation (D_2O-H_2O) in SANS measurements reveals clear similarity in the structural organizations of nucleic acids (NA) and proteins. Both chromatin components show bifractal behavior with logarithmic fractal structure on the large scale and volume fractal with slightly smaller than 2.5 structure on the small scale. Scattering intensities from chromatin, protein component, and NA component demonstrate an extremely extensive range of logarithmic fractal behavior (from 10^{-3} to approximately 10^{-1} nm^{-1}). We compare the fractal arrangement of rat lymphocyte nuclei with that of chicken erythrocytes and the immortal HeLa cell line. We conclude that the bifractal nature of the chromatin arrangement is inherent in the nuclei of all these cells. The details of the fractal arrangement—its range and correlation/interaction between nuclear acids and proteins are specific for different cells and is related to their functionality.

DOI: 10.1103/PhysRevE.104.064409

I. INTRODUCTION

In spite of the great interest in the question of how the chromatin is arranged and structured in the nuclei of a biological cell, its structural features remain unknown. It is related to the fact that its organization changes permanently in the course of the cell life cycle. Moreover its structure is not as trivial as periodic, neither it is homogeneous in density at different scales from nanometers to microns. So it is natural to suppose that the structure has the hierarchical and possibly fractal character [1]. Nowadays investigations are focused not only on finding the relationship between chromatin fractal structure and biological functions [2], but scientists pretend to distinguish the fractal chromatin architecture of a normal biological cell from that of a cancer cell [3,4].

The fractal-based three-dimensional (3D) simulations of DNA packaging in the chromatin may explain how very long macromolecules can be unpacked without entanglement [5–11]. Dynamic simulations of thermal motion of monomers forming a fractal polymer structure show that the self-diffusion in such a structure is much faster than in the equilibrium tangled globule [12]. Based on imaging studies and simulations, a model of large-scale chromatin folding was proposed: The topologically associated domains are liquid-tree-like structures, linked and isolated by stretched-out, transcriptionally active DNA to form a secondary structure of chromatin that further folds into a "3D forest" under confinement [13].

Small-angle neutron scattering is one of the most informative and direct ways to study the chromatin structural organization on nano- and microscales. The scattering intensity $I(Q)$ is related to fluctuations in the scattering density $\rho(r)$ and is equal to the Fourier transform of the correlation function of the object $\gamma(r)$. The self-similarity of a fractal object is converted to the power law of scattering intensity [14,15]. This ability of the SANS method to characterize the internal structure of the nano-object can be strengthened by use of the D_2O-H_2O contrasting technique that is used to reveal scattering on one of two parts in two-component systems. This advantage of the SANS technique is often used in studies of chromatin consisting of nucleic acids (NA) and proteins.

One of the most modern and perspective hypothesis about universal principle of large-scale organization of interphase chromatin is bifractal organization with logarithmic fractal structure on the largest scales and mass fractal structure with the dimension slightly less than 2.5 on the smaller scales. This hypothesis on the chromatin organization was experimentally proven by small-angle neutron scattering (SANS) on the nuclei of chicken erythrocytes [16–18] and HeLa cells [19–21]. Moreover, use of the contrast variation technique in small-angle neutron scattering allows one to study separately the structure of the chromatin components (NA and proteins) as well as to see their correlations, if the components are intertwined [21].

As was reported in [16] for the chromatin in chicken erythrocyte nuclei contrasted by the 100% of D_2O, the exponent

D of the power function Q^{-D} in the Q dependence of SANS intensity equals 2.4 on the scale of 15–400 nm, and it is 2.9 (i.e., close to 3) on the scales from 400 to 1500 nm. The neutron scattering technique (with the help of D_2O-H_2O contrasting) was used to separate the contribution of the DNA architecture that also exhibited two different regimes of fractality with a $D = 2.2$ exponent in 15–400 nm spatial range and $D = 3.2$ exponent for larger length scales. As to the nuclear protein organization, it is found to associate with a fractal behavior with an exponent of 2.4 over the full length spectrum. In the framework of the fractal concept $D = 2.4$ corresponds to the mass fractal with the fractal dimension $D_F = 2.4$. The exponent close to 3 was interpreted as the very special type of fractal organization of matter—the logarithmic fractal [15,17,19].

In contrast to synthetically inactive chicken erythrocyte nucleus, the Hela cell line is often chosen for the studies as an actively dividing cell line [22–24]. The SANS study of the chromatin structure of the interphase HeLa nuclei has been recently performed in the Q range spanning from the nucleosome size (∼10 nm) to the nucleus (∼6000 nm) [19]. It was shown that the small-scale structure corresponds to mass fractal with dimension $D_F = 2.41$ on the scale from 9 to 80 nm. While the large-scale organization corresponds to logarithmic fractal ($D = 3$) on the scale from 80 to 5100 nm.

The detected exponents in the power law of scattering intensity from the HeLa nuclei are similar to those from chicken erythrocyte nuclei [17,19] which supports the general hypothesis of the bifractal structure of chromatin in the interphase nuclei. The mass fractal is self-similar at different scales, while the logarithmic fractal is hierarchically changed upon scaling [17]. As a result the logarithmic fractal is more compact than the volume fractal, but it still has a rather high surface area, which provides accessibility at all length scales. Apparently, such bifractal chromatin organization is the result of an evolutionary process of optimizing the compactness and accessibility of gene packing. The small-scale mass fractal organization is built to satisfy the necessity of protein diffusion, while the large-scale logarithmic fractal is formed under the influence of two factors: protein diffusion and gene transcriptional activity.

The logarithmic fractal in the HeLa nuclei covers two orders of magnitude in scale while the mass fractal spreads for one order only. In the nuclei of the chicken erythrocytes it is exactly the opposite: The logarithmic fractal occurs within one order of the large-scale chromatin architecture but the volume fractal spreads for two orders of magnitude in scale. Probably, this difference is related to the fact that the chicken erythrocyte nucleus is dormant (there is an insignificant transcription process and no replication) while in the HeLa nucleus there are intense replication and transcription processes. It may be assumed that the DNA and proteins intertwine strongly and interacts actively in the HeLa nuclei while these two components of chromatin in chicken erythrocytes are less interconnected and do not interact.

The present work focuses on the nuclei of actively functioning but nondividing cells—the rat lymphocyte. In typical life process lymphocytes produce specific proteins (antibodies, cytokines, etc.) to protect organism from foreign bodies. The main goal of lymphocyte is to ensure the organism's immunity but not self-reproduction, thus lymphocyte is normally nondividing cell functioning actively in the life process. Opposite to the chicken erythrocyte nucleus, this nucleus is not dormant, since active transcription occurs in the nucleus throughout the lymphocyte life. Thus it is of great interest to study the chromatin structural arrangement of the rat lymphocytes and compare it to that of the chicken erythrocytes and actively dividing HeLa cell.

The paper is organized in the following way. Section II represents the description of sample preparation and AFM measurements of the rat lymphocyte nuclei. The experimental data of the SANS measurements using contrast variation technique and its appropriate data interpretation is given in Sec. III. The comparative analysis of the chromatin structure of the three different cells and conclusion are given in Secs. IV and V.

II. SAMPLES PREPARATION

Lymphocytes were isolated from the spleen, which was in the Versen solution (PBS buffer with 3 mM EDTA), by mechanical treatment. The resulting suspension of lymphocytes in Versen solution was carefully layered on 5 ml of sterile ficoll (the density was $1.130\,g/cm^3$) and centrifuged for 15 min at 170 rpm. A layer of lymphocytes was selected with a pipette and drained into a test tube with a serum-free nutrient medium. The obtained lymphocytes were washed twice in Versen solution by centrifugation to completely remove ficoll.

The resulting spleen cells are lysed within 5 min with 0.1% Triton-X100 in culture medium DMEM/F12 with 15 mM Hepes. Then nuclei were fixed by 0.5% glutaraldehyde within 10 min and washed from glutaraldehyde by centrifugation. The resulting precipitate was resuspended in PBS. We also centrifuged the part of the nuclei disposed as a thin layer on a glass prior fixation in order to check their resistance to mechanical stress. It turned out that rat lymphocyte nuclei were flattened in a centrifuge at a speed of 60 rcf.

The process of destruction of cells, separation of the nuclei, and integrity after deformation were controlled by the cytometry. The flow cytofluorimeter (Cell Lab Quanta SC by Beckman Coulter) was used to analyze properties of nuclei. Cell nuclei for analysis performed at a flow cytometer were stained with Hoechst 33342 (Sigma) fluorescent dye at a concentration of $10\,\mu g/ml$. This dye specifically binds exclusively to DNA in its native form along the minor groove. In our research, it is used at saturation concentration. The fluorescence intensity is directly proportional to the amount of DNA in the nucleus. It can be seen from the histograms (Fig. 1) that the fluorescence intensity for all nuclei is the same in both nondeformed and deformed nuclei. Therefore, there is no loss of DNA or its destruction in the used treatments.

III. STUDY OF MECHANICAL PROPERTIES OF CHROMATIN BY ATOMIC FORCE MICROSCOPY

The characteristic sizes of the deformed by centrifugation and nondeformed nuclei were investigated using atomic force microscopy on a Solver Bio microscope (NT-MDT, Russia). The atomic force microscopy (AFM) images are shown in Fig. 2(a) for individual nucleus of the rat lymphocyte after

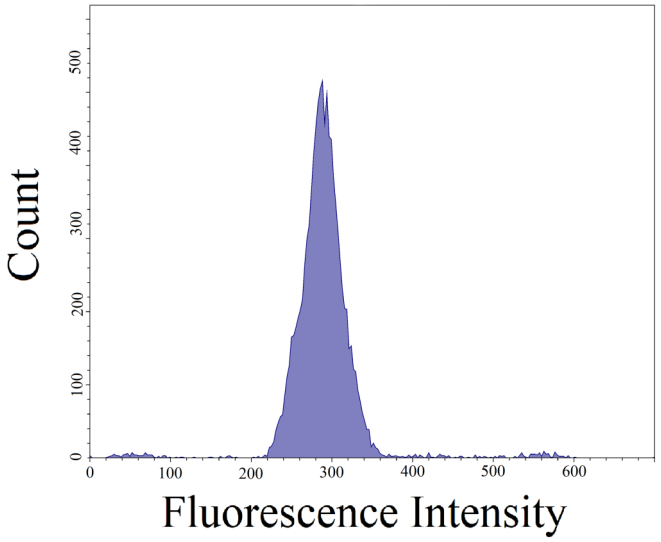

FIG. 1. Flow cytometry histograms for the sample of the rat lymphocyte nuclei.

isolation and fixation procedures with glutaraldehyde. To affect the shape of nuclei, they were disposed on a substrate and centrifuged (deformed), then fixed and rinsed [Fig. 2(b)]. A glass slide modified with 0.001% wt. poly-l-lysine was used as a substrate.

Centrifugation was carried out at 60 rcf using UNION 5KR centrifuge equipped WS750-6B swinging rotor. After rinsing with distilled water, all slides were air-dried at room temperature.

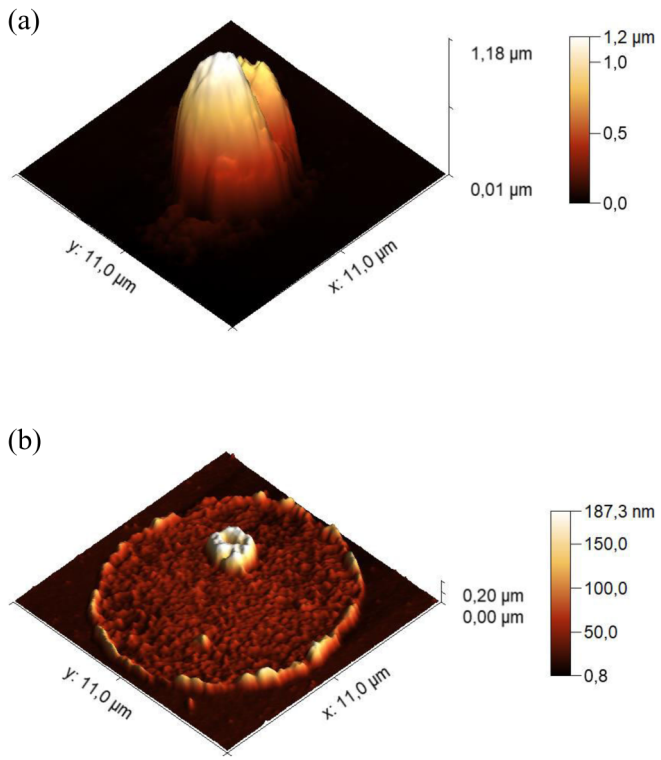

FIG. 2. Surface reliefs of the rat lymphocyte nuclei. (a) Fixed in suspension and (b) centrifuged on the substrate and then fixed.

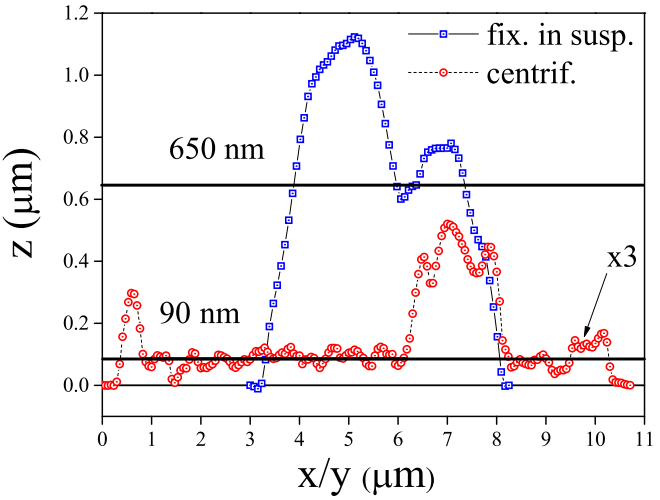

FIG. 3. The cross sections of the surface reliefs of the rat lymphocyte nuclei shown in Fig. 1 for nuclei fixed in suspension (blue squares), for nuclei fixed on the substrate, and for centrifuged (deformed) and then fixed nuclei (red circles).

The 3D visualization of nuclei disposed on the substrate in Fig. 2(a) gives an image of a buttonlike object with a few well-defined hills on its top. The width of the "button" exceeds 5 μm, while its height is less than 1.1 μm. Figure 2(b) shows what happens to the nuclei when not the gravity with 1 g but the centrifuge with 60 rcf is applied. The nuclei are squashed over some area on the substrate.

Figure 3 shows the cross sections of the surface reliefs of the nuclei shown in Fig. 2 for nucleus fixed in suspension (a) and for the centrifuged one (b). The width of the fixed in suspension nucleus is 5 μm and its height exceeds 650 nm, while the width of the centrifuged and then fixed nucleus is about 10 μm and its height is approximately 30 nm. The width and height of the small peaks are of order of 0.8-1.1 μm and 130–170 nm, respectively. The total volume of nuclei is 8.8 μm^3 before centrifugation and is 2.8 μm^3 after centrifugation, i.e., the volume changes by factor of 3.25. Thus nuclei lose three-quarters of their volumes upon centrifugation. One may assume that similar to the chicken erythrocyte nuclei the internal structure of the rat lymphocyte nuclei will dramatically change upon deformation [18]. At this moment we conclude that the nuclei is extremely soft in the whole range of sizes down to 30 nm. The structural study of the deformed rat lymphocytes nuclei with the help of SANS will the subject of a forthcoming paper.

IV. SMALL-ANGLE NEUTRON SCATTERING WITH CONTRAST VARIATION FROM LYMPHOCYTE NUCLEI

The structural study of the chromatin and its components [nucleic acids (NA) and proteins] in the isolated rat lymphocyte nuclei was carried out at the KWS-3 instrument [25] in the momentum transfer range [10^{-3}-9 $\times 10^{-2}$] nm^{-1} and at the KWS-2 instrument [26] in the momentum transfer range [9 $\times$ 10^{-2}-2] nm^{-1} at MLZ, Garching, Germany. The experiments at KWS-2 were done using, first, neutrons with wavelength $\lambda = 5$ Å at two sample-detector distances (2 and

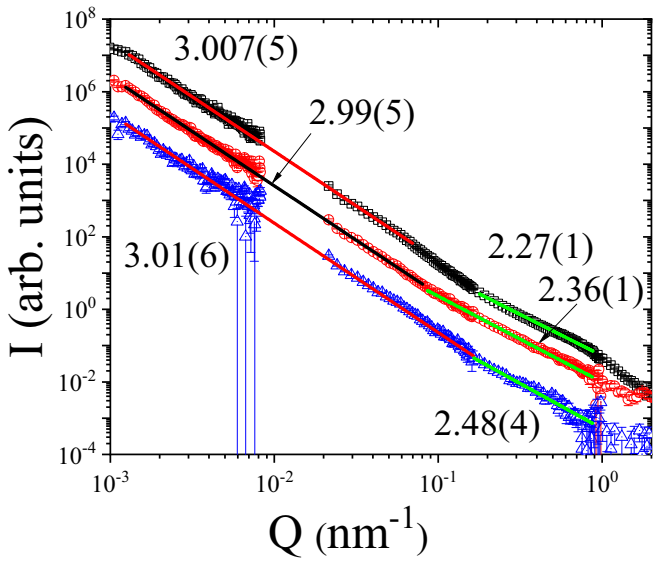

FIG. 4. Small-angle neutron scattering on the rat lymphocyte nuclei in heavy water D_2O (black open squares), in 60% D_2O ÷ 40% H_2O (red open circles), and in 40% D_2O ÷ 60% H_2O (blue open triangles).

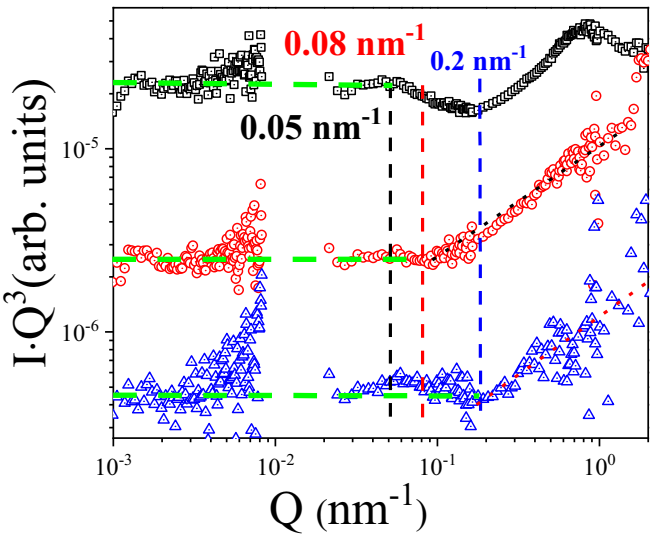

FIG. 5. Small-angle neutron scattering intensities multiplied by Q^3 taken for the rat lymphocyte nuclei in heavy water D_2O (black open squares), in 60% D_2O ÷ 40% H_2O (red open circles) and in 40% D_2O ÷ 60% H_2O (blue open triangles).

8 m) and, secondly, neutrons with wavelength $\lambda = 10$ Å at sample-detector distance 20 m. The conditions of the experiments at KWS-3 were as follows: a neutron wavelength of $\lambda = 12$ Å, a detector-sample distance of 10 m, and the neutron beam was focused by the unique toroidal mirror [25]. Both experiments were carried out with samples of the rat lymphocyte nuclei diluted in three different D_2O ÷ H_2O mixtures.

100% D_2O to get maximal contrast between chromatin and the diluting buffer and to obtain scattering pattern from all the inhomogeneities of the nuclei,

60% D_2O ÷ 40% H_2O to match the NA part ($\Delta\rho_{NA} = 0$) of the nucleus and to visualize the protein part only,

40% D_2O ÷ 60% H_2O to match the protein part ($\Delta\rho_p = 0$) and to visualize the NA part.

The resulted data were processed by the software QTIKWS [27]. The ORIGIN software was used to find the best fitted curves to data and to plot the graphs.

Figure 4 shows three scattering curves in a wide momentum transfer range [10^{-3}-2] nm^{-1}. These three orders of magnitude are in size scales from 3 nm to 6 μm, i.e., they cover the whole range of sizes inherent to nucleus. Similar to the analysis of the SANS data made in [17,19,20], we observe two fractal levels for the scattering curve taken from chromatin (100% D_2O). The curve plotted in double logarithmic scales has a clear fracture in the range from 0.05 nm^{-1} to 0.2 nm^{-1} (from 100 to 30 nm in real space). The parts of the curve on the left and on the right sides from the featured range are well described by a power function $I(Q) \sim Q^{-D}$ with the power $D = 3.007 \pm 0.005$ in the range [10^{-3}-5 × 10^{-2}] nm^{-1} and $D = 2.27 \pm 0.01$ in the range [2 × 10^{-2}-1] nm^{-1}, respectively.

The difference between the indexes observed in the different Q ranges makes one conclude that the fractal structure of the chromatin in the nucleus changes its nature upon transition from the smaller scale (tens of nanometers) to the larger scale (hundreds of nanometers). The correlation function of the object, characterized by the scattering law of Q^{-D} with $2 < D < 3$, is described by the expression: $\gamma(r) \sim (r/\xi)^{D-3}$ and corresponds to a mass fractal of the dimension D. With D approaching to 3, the correlation function changes its nature and can be described by the ratio: $\gamma(r) \sim \ln(\xi/r)$. The change of the nature of the correlation function leads to the fundamental change of the properties and structure of chromatin in the cell nucleus [15,17].

Similar curves with the same bifractal structure are observed for proteins (nuclei in mixture 60% D_2O ÷ 40% H_2O) and for NA (nuclei in mixture 40% D_2O ÷ 60% H_2O) (Fig. 4). These two curves show the power dependence Q^{-D} with $D = 2.36 \pm 0.01$ in the range of [$8 \cdot 10^{-2} - 1$] nm^{-1} for the proteins and with $D = 2.348 \pm 0.04$ in the range of [$2 \times 10^{-1} -$ 1] nm^{-1} for the NA. Both curves show very similar cubic dependencies in the range of small Q: $D = 2.99 \pm 0.05$ in the range of [10^{-3}-8 × 10^{-2}] nm^{-1} for the proteins and with $D = 3.01 \pm 0.06$ in the range of [10^{-3}-2 × 10^{-1}-1] nm^{-1} for the NA.

To better visualize the crossover points in the three curves and to emphasize the cubic dependence, we plotted them multiplied by Q^3 in Fig. 5. It is important to note that the scattering intensities from NA and proteins have two different crossover points ($Q_{NA} = 0.2$ nm^{-1} and $Q_p = 0.08$ nm^{-1}), while the curve from whole chromatin demonstrates rather wide fracture interval from 0.05 nm^{-1} to 0.2 nm^{-1} (Fig. 5). One concludes that both NA and proteins have slightly different mass fractal arrangements on the scale from 6 to 60 nm and in the same time very similar logarithmic fractal arrangement on the scale from 100 to 6000 nm.

The superposition (linear combination with weight) of two scattering curves from NA and proteins never gives a scattering curve from whole chromatin. Often these two components are interconnected and even intertwined in larger or smaller extent at the different scales from nano- to micrometers. As a

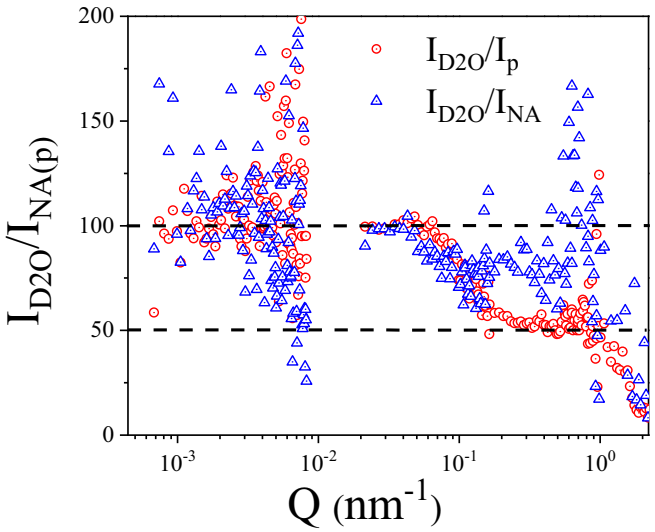

FIG. 6. Ratio of intensities $R_{NA(p)} = I_{D2O}/I_{NA(p)}$ for the sample with D_2O and for those with the mixtures (60% D_2O + 40% H_2O) and (40% D_2O + 60% H_2O) for the rat lymphocyte nuclei.

result the interference scattering (the cross term between NA and proteins) arises and adds not negligible contribution to the curve from chromatin [21].

Based on the striking similarity of the three curves in the region of small momentum transferred Q, we can conclude that DNA and proteins have the same structure on scales from 10 to 3000 nm, that is, in the region where the Q^{-3} law is observed. Moreover, the same structure of two chromatin components implies their interconnection and most probable submittance of protein structure to one of NA. The differences observed in the range of large Q can be interpreted in terms of at least partial independence of proteins and NA structures. The interference contribution and the correlation between NA and protein structures can be extracted by comparison of the intensities for the sample with D_2O buffer and for those with the mixtures (60% D_2O + 40% H_2O) and (40% D_2O + 60% H_2O) as a buffer taken in the wide q range. This ratio $R_{NA(p)} = I_{D2O}/I_{NA(p)}$ normalized to 100 in the small Q range is shown in Fig. 6.

As can be seen from Fig. 6, the ratio is constant (normalized to 1) for both mixtures with 60% D_2O and 40% D_2O in the whole Q range with the logarithmic fractal characteristics from 10^{-3} nm^{-1} to roughly 10^{-1} nm^{-1}. Remarkable that the ratio decreases to smaller levels in the momentum transfer range above the crossover points $Q_{NA(p)} = 0.08$ nm^{-1}, i.e., in the mass fractal range. The level of ratio R_{NA} for the large Q is by factor of 0.8 smaller than in the low Q range for the NA, while R_p for the high Q is by factor of 0.5 smaller than in the low Q range for the proteins. This lack of the intensity in the chromatin curve (100% of D_2O) implies absence of the interference in scattering between proteins and NA and as such lack of correlations between them. It is most probable that we observe large uncorrelated to NA contribution of the protein part.

The strong interconnection of the components of chromatin on the large scales of its structure and lack of their correlation on the small scales is remarkable itself but it also allows one to assume that two fractal structures have independent mechanisms and different nature. The small fractal structure (the mass fractal) grows from atomic scale to a superstructure as the diffusion limited aggregate (DLA) object that is well known in the fractal science [28]. In most cases it is possible even to reproduce the DNA mass fractal structure in computer modeling [29,30]. The large fractal structure (the logarithmic fractal) grows from the nucleus size down to tenths of nanometers that is in the opposite to the mass fractal direction. It is most probably determined by the equilibrium between the maximum availability of any section from the outside and most compact, dense structure allowing active interactions between different parts of genes.

V. COMPARISON OF THE CHROMATIN ARRANGEMENT IN DIFFERENT CELLS

Before coming to final conclusions it is instructive to make comparative analysis of the results of SANS experiments obtained on the rat lymphocyte nuclei and those of chicken erythrocytes [16–18] and HeLa nuclei [19,21]. The available set of the SANS experiments clearly demonstrates that chromatin in the nuclei of the three different cells has the bifractal nature with two organizational levels: the mass fractal arrangement at smaller scale and the logarithmic fractal arrangement at larger scale. It makes us conclude that the bifractal structure is the generic feature of the chromatin and, particularly DNA, arrangement in nuclei of any cell. However, this is all one can say on the similarities of the nucleus structure because the details of structural arrangement are very different. Many small details of the structure describe nuclei with very specific features inherent in this particular cell under study.

In spite of the fact that rat lymphocytes and chicken erythrocytes are both nondividing cells, the structural arrangement of chromatin in their nuclei is fantastically different. The logarithmic fractal level for chicken erythrocyte cover a small range of less than an order of magnitude (from 500 to 3000 nm [17]) while for the rat lymphocytes it spans for more than two orders (from 10 to 3000 nm). Moreover, the logarithmic fractal structure is observed for the DNA only in chicken erythrocyte nuclei but the proteins are arranged in the mass fractal structure at any scale. Different arrangements of the DNA and proteins in the nuclei of chicken erythrocytes makes us assume that the two chromatin components are not correlated in the nuclei and most probably they do not interact. Such nonactive, uncorrelated structure is naturally expected for the sleeping (dormant) nuclei of the chicken erythrocytes. The chromatin components in the rat lymphocyte nuclei demonstrate strong similarities, connection and, most probably, interactions in the wide range of scales.

The comparison of the rat lymphocyte nuclei with those of the HeLa cells shows more similarities in their structures. They both have bifractal arrangements for the NA and proteins with the very large range of the logarithmic fractal and rather limited range of the mass fractal from 10 to 100 nm. We conclude that the active cells—no matter if they are actively dividing like HeLa, or are active in production of the proteins—possess the large range of the logarithmic fractal structure. This logarithmic fractal range develops from the low

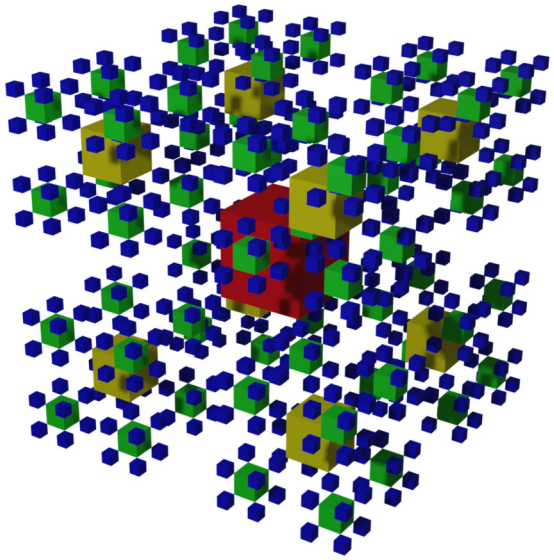

FIG. 7. The fourth generation logarithmic fractal built on the basis of cubes in 3D space is considered as a preliminary model for the large-scale organization of chromatin.

q (size of nuclei) to large q (single molecule size) with the aim to provide high accessibility agents to specific gene site that gives facilitated diffusion of external proteins in chromatin. The two cells under comparison, however, demonstrate remarkable difference. In contrast to scattering intensities from HeLa nuclei that have precise crossover points between two fractals for NA and proteins, scattering intensity from rat lymphocyte nuclei demonstrated a blurry crossover point (or crossover area) that spreads from 0.05 nm^{-1} to 0.2 nm^{-1} (from 100 to 30 nm in real space). The smeared crossover in the chromatin curve is caused by the two distinct crossovers in the curves for the NA and proteins found in the rat lymphocyte nuclei. We conclude that in contrast to the Hela nuclei the protein and NA structures in the rat lymphocyte nuclei are weakly correlated at the scales of 10–100 nm. To strengthen the diversity of two cells, we note that the NA and proteins lose their correlations at a scale of a few microns in the Hela nuclei, which is not observed in the rat lymphocyte nuclei. This lack of correlation in the Hela nuclei at micron scale is explained by necessity of the cell to follow the dividing life cycle, which is not functioning in the rat lymphocyte nuclei.

In all three cases we correlate these crossover points, corresponding to few tens or hundreds of nanometers in the direct space, with the size of the solid part of the chromatin obtained in the AFM measurements. We speculate that they are the very same objects inside the nuclei that form the mass fractal arrangement and to resist stresses induced by centrifugation upon sedimentation of nuclei on the substrate.

VI. CONCLUDING REMARKS

Based on the comparison of the structural arrangements of nuclei of three different cells one can come to more general conclusions or, at least, formulate several hypotheses.

For the rat lymphocytes nuclei, the DNA and proteins are correlated in logarithmic fractal range, and the correlation is lost on the smaller scales coinciding with the mass fractal structure. The borderline between two fractal structures is detected at tens of nm which may correspond to transcriptional activity areas associated with synthesis that is specific for each lymphocyte protein. Absence of a replication process in this cell results in the high correlation between NA and proteins on large scales, which is a consequence of structural packing.

The terms and concepts of ontogenesis and phylogenesis are usually applied to individual organisms and to species, respectively. Ontogenesis is the process of individual development of an organism from the moment of its formation to the natural completion of its life cycle, while phylogenesis is evolutionary development of a species, i.e., the historical development of living organisms, the formation, separation, and extinction of taxa. We may conclude that the bifractality of the chromatin structure is a result of the phylogenesis because is is observed in different nuclei of eukaryotes, including the dormant chicken erythrocyte nuclei. On the other hand, the "size" of logarithmic fractal (range of scales where the fractal exists) determines the specificity and degree of functioning of the cell and as such is related to ontogenesis. We see that although the bifractal structure of the chromatin arrangement is the generic property of the nucleus of eukaryote, the other features such as scale range of two different fractals and the strong or weak correlation between DNA and proteins, are specific to the individual cell line. These features are related to the current functions of the concrete cell.

Since the logarithmic fractal at large scales and mass fractal for small scales are observed for chromatin arrangement of the three cells, one can conclude that the two different principles and two different mechanisms are involved in the realization in the two different chromatin arrangements. One mechanism of the mass fractal at relatively small scale is realized through DLA principle. This mechanism implies the growth of the fractal using "small-to-big" principle having the small molecules as building blocks. One may note that it is of "chemical" nature. Another mechanism of the logarithmic fractal ensures the maximum availability of any section from the outside and most compact displacement of chromatin. The equilibrium between two tendencies was found in the evolutionary process of life. Building of this fractal starts from the large element using "big-to-small" principle and grows splitting it to the number of small elements; those in turn split into the same number of smaller ones (the so-called Leonardo da Vinci principle for the botanical tree [31,32]).

In analogy to the Leonardo da Vinci principle for two-dimensional space [31,32], we imagine the logarithmic fractal in the 3D space using the principle of volume conservation upon changing scale. The (homogeneously filled) cube in the center is surrounded by eight cubes with the linear size of one-half the previous one; those in their turn are surrounded by eight smaller cubes with the linear size of one-half the previous cubes, etc. Please note that all cubes are homogeneously filled with matter. The number of generations is directly related to the scaling range of the logarithmic fractal. Thus, the third generation logarithmic fractal would satisfy

the experimental SANS picture for the chicken erythrocytes, while one has to consider the seventh generation logarithmic fractal for the rat lymphocytes. Visualization of the fourth generation logarithmic fractal in three dimensions is presented in Fig. 7. Please note that cubes can be replaced by spheres and the form of the building element does not change the relevance of the model. We warn the reader that this picture is only a preliminary model of the logarithmic fractal that satisfies its principles and the cubic decay in the Q dependence in the SANS data. A picture of the chromatin organization in the biological cell deserves separate, deep, comprehensive study.

ACKNOWLEDGMENTS

We would like to thank the neutron center MLZ for the beamtime allocation and K. A. Pschenichnyi for the visualization of the logarithmic fractal in 3D space. This work is supported by the Russian Science Foundation (Grant No. 20-12-00188).

[1] A. Bancaud, C. Lavelle, S. Huet, and J. Ellenberg, Nucleic Acids Res. **40**, 8783 (2012).
[2] L. M. Almassalha, A. Tiwari, P. T. Ruhoff, Y. Stypula-Cyrus, L. Cherkezyan, H. Matsuda, M. A. Dela Cruz, J. E. Chandler, C. White, C. Maneval, H. Subramanian, I. Szleifer, H. K. Roy, and V. Backman, Sci. Rep. **7**, 1 (2017).
[3] K. Metze, Expert Rev. Mol. Diagn. **13**, 719 (2013).
[4] K. Metze, R. Adam, and J. B. Florindo, Expert Rev. Mol. Diagn. **19**, 299 (2019).
[5] L. A. Mirny, Cromosome Res. **19**, 37 (2011).
[6] V. A. Avetisov, V. A. Ivanov, D. A. Meshkov, and S. K. Nechaev, Biophys. J. **107**, 2361 (2014).
[7] A. Rosa and R. Everaers, Phys. Rev. Lett. **112**, 118302 (2014).
[8] A. Rosa and Ch. Zimmer, Inter. Rev. Cell Mol. Bio. **307**, 275 (2014).
[9] J. Dekker, M. A. Marti-Renom, and L. A. Mirny, Nat. Rev. Genet. **14**, 390 (2013).
[10] J. Nuebler, G. Fudenberg, M. Imakaev, N. Abdennur, and L. A. Mirny, PNAS **115**, E6697 (2018).
[11] W. Schwarzer, N. Abdennur, A. Goloborodko, A. Pekowska, G. Fudenberg, Ya. Loe-Mie, N. A. Fonseca, W. Huber, Ch. H. Haering, L. Mirny and F. Spitz, Nature (London) **551**, 51 (2017).
[12] M. V. Tamm, L. I. Nazarov, A. A. Gavrilov, and A. V. Chertovich, Phys. Rev. Lett. **114**, 178102 (2015).
[13] K. Huang, V. Backman, I. Szleifer, bioRxiv:413872.
[14] J. Teixeira, J. Appl. Crystallogr. **21**, 781 (1988).
[15] E. G. Iashina and S. V. Grigoriev, J. Surf. Sci. Technol.: X-ray, Synchrotron and Neutron Techniques **11**, 897 (2017).
[16] D. V. Lebedev, M. V. Filatov, A. I. Kuklin, A. Kh. Islamov, E. Kentzinger, R. Pantina, B. P. Toperverg, and V. V. Isaev-Ivanov, FEBS Lett. **579**, 1465 (2005).
[17] E. G. Iashina, E. V. Velichko, M. V. Filatov, W. G. Bouwman, C. P. Duif, A. Brulet, and S. V. Grigoriev, Phys. Rev. E **96**, 012411 (2017).
[18] S. V. Grigoriev, E. G. Iashina, V. Yu. Bairamukov, V. Pipich, A. Radulescu, M. V. Filatov, R. A. Pantina, and E. Yu. Varfolomeeva, Phys. Rev. E **102**, 032415 (2020).
[19] E. G. Iashina, M. V. Filatov, R. A. Pantina, E. Yu. Varfolomeeva, W. G. Bouwman, Ch. P. Duif, D. Honecker, V. Pipich, and S. V. Grigoriev, J. Appl. Crystallogr. **52**, 844 (2019).
[20] E. G. Iashina and S. V. Grigoriev, J. Exp. Theor. Phys. **129**, 455 (2019).
[21] S. V. Grigoriev, E. G. Iashina, B. Wu, V. Pipich, Ch. Lang, A. Radulescu, V. Yu. Bairamukov, M. V. Filatov, R. A. Pantina, and E. Yu. Varfolomeeva, Phys. Rev. E **104**, 044404 (2021).
[22] G. S. Miglani, *Developmental Genetics* (I. K. International Publishing House, New Delhi, 2006).
[23] Y. Nishino, M. Eltsov, Y. Joti, K. Ito, H. Takata, Y. Takahashi, S. Hihara, A. S. Frangakis, N. Imamoto, T. Ishikawa, and K. Maeshima, EMBO Journal **31**, 1644 (2012).
[24] Y. Joti, T. Hikima, Y. Nishino, F. Kamada, S. Hihara, H. Takata, T. Ishikawa, and K. Maeshima, Nucleus **35**, 404 (2012).
[25] V. Pipich and Z. Fu, Journal of large-scale research facilities (JLSRF) **1**, 31 (2015).
[26] A. Radulescu, N. K. Szekely, and M. S. Appavou, Journal of large-scale research facilities (JLSRF) **1**, 29 (2015).
[27] Computer program QTIKWS: user-friendly program for reduction, visualization, analysis and fit of SA(N)S data https://www.qtisas.com/.
[28] J. Feder, *Fractals* (Plenum, New York, 1998).
[29] A. V. Ilatovskiy, D. V. Lebedev, M. V. Filatov, M. Grigoriev, M. G. Petukhov, and V. V. Isaev-Ivanov, J. Appl. Phys. **110**, 102217 (2011).
[30] A. V. Ilatovskiy, D. V. Lebedev, M. V. Filatov, M. G. Petukhov, and V. V. Isaev-Ivanov, J. Phys.: Conf. Ser. **351**, 012007 (2012).
[31] J. P. Richter and R. C. Bell, *The Notebooks of Leonardo da Vinci* (Dover, New York, 1970).
[32] J. O. Indekeu and G. Fleerackers, Phys. A **261**, 294 (1998).